Available online at www.sciencedirect.com
SCIENCE DIRECT®
ELSEVIER
Nuclear Instruments and Methods in Physics Research A 517 (2004) 313–336
NUCLEAR INSTRUMENTS & METHODS IN PHYSICS RESEARCH Section A
www.elsevier.com/locate/nima

Temperature characterization of deep and shallow defect centers of low noise silicon JFETs

Claudio Arnaboldi[a], Andrea Fascilla[a], Mark W. Lund[b], Gianluigi Pessina[a,*]

[a] *Dipartimento di Fisica, INFN, Istituto Nazionale di Fisica Nucleare, Università degli Studi di Milano-Bicocca, P. za della Scienza 3, Milano 20126, Italy*

[b] *Lund Instrument Engineering, Inc., 140 South Mountainway Drive, Orem UT 84058, USA*

Received 10 January 2003; received in revised form 4 September 2003; accepted 5 September 2003

Abstract

We have selected different low noise JFET processes that have shown outstanding dynamic and noise performance at both room temperature and low temperatures. We have studied JFETs made with a process optimized for cryogenic operation, testing several devices of varying capacitance. For most of them, we have been able to detect the presence of shallow individual traps at low temperature which create low frequency (LF) Generation–Recombination (G–R) noise. For one device type no evidence of traps has been observed at the optimum temperature of operation (around 100 K). It had a very small residual LF noise. This device has been cooled down to 14 K. From below 100 K down to 14 K the noise was observed to increase due to G–R noise originating from donor atoms (dopants) inside the channel. A very simple theoretical interpretation confirms the nature of G–R noise from these very shallow trapping centers. We also studied devices from a process optimized for room temperature operation and found noise corresponding to the presence of a single deep level trap. Even for this circumstance the theory was experimentally confirmed. The measurement approach we used allowed us to achieve a very high accuracy in the modeling of the measured G–R noise. The ratio of the density of the atoms responsible for G–R noise above the doping concentration, N_T/N_d, has been verified with a sensitivity around 10^{-7}.

PACS: 07.50.−e; 07.50.Ek; 07.50.Yd; 84.30.−r; 84.30.Le; 84.30.Yq; 85.30.De; 85.30.Tv; 85.40.Qx

Keywords: Low noise transistors; Noise; Low temperature operation; Cryogenic electronics; JFET

1. Introduction

There is a large demand for devices to be operated at low temperature, having both low series noise at low frequency (LF) and low parallel noise. One class of applications, from which this work was started, is bolometers [1], which are large impedance detectors [2] that generate slow signals and are able to reach very high energy resolution [3].

A systematic study and selection of transistor properties has been made for the readout of bolometric detectors for two requirements: the first stage (located at cryogenic temperature) and the second stage (located at room temperature). Silicon JFETs have been investigated for both

*Corresponding author. Tel.: +39-02-644-82825; fax: +39-02-644-82463.

E-mail address: pessina@mib.infn.it (G. Pessina).

0168-9002/$ - see front matter © 2003 Elsevier B.V. All rights reserved.
doi:10.1016/j.nima.2003.09.034

cases since they have superior low frequency and parallel noise performances.

The study and interpretation of G–R noise is also important for applications where the devices operate in the presence of radiation [4,5] such as space applications or experiments that make use of particle accelerators.

In this paper, we present the results obtained in the selection of a transistor process optimized for cryogenic operation and a transistor process optimized for room temperature operation. Accurate investigation has been made with regards to the LF region of the noise spectra. Since the transistors selected showed very outstanding performances, a very accurate investigation was possible that confirmed the G–R nature of noise coming from individual traps. At very low temperatures the noise limit of silicon JFETs was proven to be due to G–R noise coming from the dopant atoms acting as traps. An analysis was developed for interpreting the measured data.

Two different set ups were used for temperature characterization. JFETs optimized for room temperature operation were measured inside an environmental chamber. The temperature was varied from -60°C to $+70^{\circ}$C.

To implement a setup for systematic transistor characterization at cryogenic temperatures, we have developed a special apparatus that is able to cool the transistors without the need of any pumping system. This was found necessary for precise characterization of the low frequency region of the noise spectra measured. The noise of the Device transistor Under Test (DUT) was readout by an amplifier with well-characterized low noise performance, that was possible to subtract from the overall noise measured. The collected data has been analyzed with fitting algorithm based on the χ^2 technique.

In the following section, the analysis of the expected noise behavior is performed. Then the cryogenic system and second amplifier stage will be addressed, including the selection of an input transistor with no G–R noise at low frequencies. In Sections 4–7 the experimental results of the low temperature noise measurement of the selected transistors will be shown in detail.

2. The analysis of LF noise coming from deep and shallow traps

Low frequency (LF) noise coming from the trapping mechanism has been extensively studied. In this paper, we will study the noise originated from the trapping centers located deep in the band gap and detail the theory for the factors affecting the shallow level centers, specifically the donor sites, at very low temperature. We have selected very low noise silicon JFET transistors to prove the theories experimentally. A very high accuracy has been reached thanks to the very low noise levels measured, around and below $1\,\mathrm{nV}/\sqrt{\mathrm{Hz}}$ at both room temperature and low temperature, obtaining high sensitivity in the temperature dependence of the trapping centers. Although at very low temperature LF noise from dopant sites has a large frequency corner, we will show that it is possible to detect it and we will prove its effects on the noise performance.

It has to be considered that other mechanisms may generate LF noise [6] that are not found to operate in the transistors we have selected. In addition, G–R noise manifests itself with different frequency behaviors (typically f^{-1} slope) in some devices (typically MOS transistors). In those cases electrons can tunnel into the oxide that is located above the channel, remaining trapped for a time that depends on how deep the tunnelling path was [7,8]. Extensive study has been done on the mechanism responsible for LF noise in MOS transistors [9–11].

The behavior of the G–R process is interpreted with the principle of the 'detailed balance' [12–14], which states that at thermal equilibrium the net rate of capture of electrons (holes), from/to the conduction (valence) band, must balance the net rate of generation of electrons (holes). After any external perturbation of this situation, the system relaxes again to the equilibrium condition. This happens with a time dependence that is related to the kind of G–R centers that are involved in the process. We are interested in how noise is generated from this stationary condition. Charge carriers can make transitions from/to the trapping centers after having absorbed/released at random energy from/to the lattice, at temperature T.

Although the detailed balance is maintained on the average since T is stationary, if a current is flowing into the device, instantaneous changes of its value will happen as a consequence of the random process of trapping/de-trapping of charges from the centers, filled around the stationary state, generating noise signals. In the time domain these processes are given by the indistinguishable superimposition of many square pulses. Nevertheless, under certain conditions, these pulses are visible and known as 'Random Telegraph Signals', RTS [15–17]. A trapping/de-trapping of a single charge results in current pulses. Let us try to quantify it. In an n-region of a semiconductor where a current is flowing, we can write:

$$I = enA\mu\frac{V_{\mathrm{BIAS}}}{L} = eN_{\mathrm{TOT}}\mu\frac{V_{\mathrm{BIAS}}}{L^2} \quad (1)$$

where A is the cross-section, L the sample length and V_{BIAS} the applied bias voltage. If a charge is freed from a trap the total number of charges N_{TOT} will change. In a simplified form, we approximate this process by $N_{\mathrm{TOT}} \to N_{\mathrm{TOT}} + 1$. Consequently [18]:

$$\Delta I = \frac{I}{N_{\mathrm{TOT}}} = \frac{I}{nAL} \quad (2)$$

the current change due to a single charge is measurable if it is larger than the peak-to-peak noise. From the above equation this is verified when the charge concentration and/or the device are very small. An example of the above interpretation is shown in Fig. 1. There the parallel noise of a small Heterojunction Bipolar Transistor at 4.2 K temperature is developed across 100 kΩ resistor and is amplified a factor of 10,000 V/V. A few nA pulses are clearly visible above the noise floor.

The noise coming from a single event is not always visible and can be complicated by its location inside the sample. The mathematical description of the G–R noise mechanism for a general case is simple when a single kind of G–R center dominates the process. When different types of G–R centers are present the overall effect can be derived by the superimposition of the noise contribution of each center, once a certain degree of correlation is taken into account. The interpretation of the measurement is more complicated in this case, although for two or three trapping centers some evaluation can be made [19–21].

The model for the G–R noise of a single level can be derived starting from the following

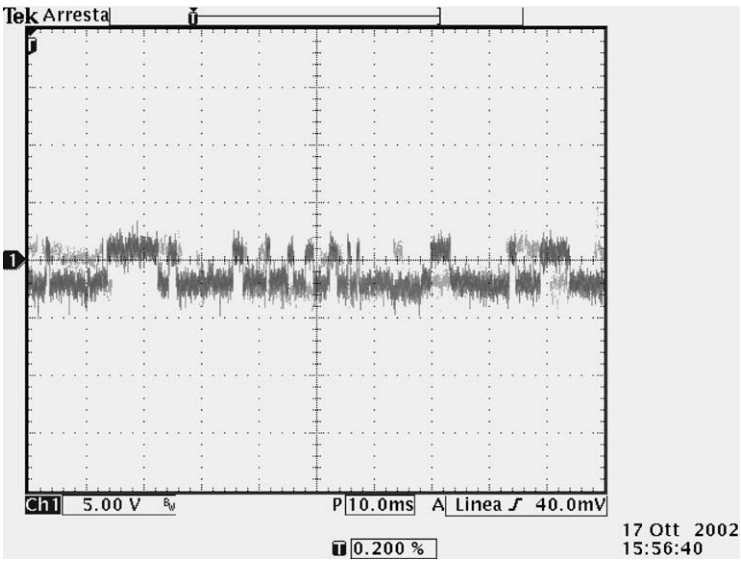

Fig. 1. RTS noise developed across 100 KΩ resistor by the parallel noise of a SiGe Heterojunction Bipolar Transistor at 4.2 K temperature. The noise has been amplified 10,000 V/V. Horizontal scale is 10 ms/div, vertical scale is 5 V/div.

law [22–25]:

$$\frac{dn_T}{dt} = (c_n n + e_p)N_T - (c_n n + c_p p + e_n + e_p)n_T - h(t). \quad (3)$$

In the above equation dn_T/dt is the rate of change of the concentration n_T (atoms/cm^3) of electrons present at the trapping centers, whose concentration is N_T, after a small perturbation, $h(t)$, is supposed to be given to the sample. n and p are the concentration of free electrons in the conduction band and free holes in the valence band, respectively. The rate of change of n_T depends on the probability $c_n(N_T - n_T)n$ that an electron is captured, the probability $e_n n_T$ that is emitted and the corresponding $e_p(N_T - n_T)$ and $c_p n_T p$ of the hole emission and capture, respectively.

Assuming that $h(t)$ is short enough, the application of the detailed balance concept, $(dn_T/dt)|_{t=\infty} = 0$, allows that:

$$\frac{dn_T}{dt} = [c_n n + c_p p_1]N_T - [c_n(n + n_1) + c_p(p + p_1)]n_T - h(t) \quad (4)$$

where

$$e_n = c_n \frac{N_T - n_{T_0}}{n_{T_0}} n_0 = c_n n_1,$$

$$e_p = c_p \frac{n_{T_0}}{N_T - n_{T_0}} p_0 = c_p p_1 \quad (5)$$

where n_0, p_0 and n_{T_0} are steady-state concentrations.

In Eqs. (4) and (5) the functions n, p and n_T are not necessary independent. The cases of interest are considered in the following.

2.1. G–R noise in a depletion region of a pn junction

The first interesting case is when Eq. (4) is applied to the depletion region of a pn junction. In this situation the concentration n and p reduce to negligible values. Any instant a charge is generated from a trapping center, it is swept away in a very short time, equal to the transit time across the junction. Since the depletion region is almost depleted from free carriers, only generation processes are possible, as shown in Fig. 2a,

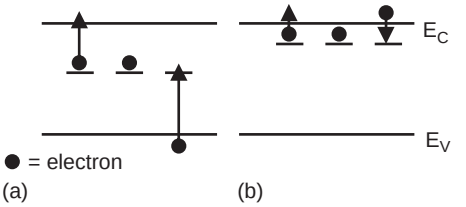

Fig. 2. (a) The more probable electron and hole emission processes from a deep trapping center in the depletion region of a reverse biased pn junction. (b) Emission and capture processes from a shallow trapping center in a forward biased pn junction. For both cases black circles represent electrons.

electrons emitted from trapping centers into the conduction band and holes emitted in the valence band, that is electrons captured from the valence band. The resulting population n_T is, therefore, independent from n_0 and p_0 and Eq. (4) can be written

$$\frac{dn_T}{dt} = [c_n n_0 + c_p p_1]N_T - [c_n(n_0 + n_1) + c_p(p_0 + p_1)]n_T - h(t). \quad (6)$$

The concentrations n_0 and p_0 strongly depend on the applied voltage in the reverse region, the concentrations being negligible at the location where the latter is at its maximum extension. Again if $h(t)$ is very short in comparison to the response time of the system, we get the following solution to Eq. (6), $h(t) \approx h_A \delta(t)$:

$$n_T(t) = [c_n n_0 + c_p p_1]\tau N_T - h_A \exp(-t/\tau)1(t)$$

$$1(t) = \begin{cases} 1 & t > 0, \\ 0 & t \leqslant 0, \end{cases} \quad \frac{d1(t)}{dt} = \delta(t) \quad (7)$$

where the time constant τ is given by

$$\tau = \frac{1}{c_n(n_0 + n_1) + c_p(p_0 + p_1)}. \quad (8)$$

In evaluating Eq. (7) no assumptions have been made in considering whether the trapping center is an acceptor or a donor. This means that it is impossible to determine the nature of the process responsible for the noise from a noise measurement.

The noise can be studied starting from Eq. (7) to which, in the frequency domain, we apply the

Wiener–Khintchine theorem:

$$\overline{\Delta n_T^2(\omega)} = \frac{\tau^2}{1+(\omega\tau)^2}\overline{h_n^2(\omega)}. \quad (9)$$

In this case the noise source is the random, temperature dependent generation/recombination of charge carriers. This random process is independent of frequency and produces a white spectrum, $\overline{h_n^2(\omega)} = \overline{h_N^2}$. The statistics that lead to its evaluation are described in Section 2.2.

Eq. (9) shows that the response to a white noise source has a Lorentzian shape.

2.2. G–R noise in a doped region

In an n-doped region, or also in a forward biased junction away from the transition region, there is a correlation between the free electrons in the n region and the trapped or emitted carriers. Since a large number of carriers are present in the conduction band, the trapping levels are active with the process indicated in Fig. 2b: capture/emission from/to the conduction band. A similar argument is valid for the holes in the p region.

When a single type of acceptor trap is dominant we have $n = N_d - n_d - n_T \approx N_d - n_T$. Eq. (4) becomes

$$\frac{dn}{dt} = c_n n_1 N_d - c_n(N_T - N_d + n_1)n - c_n n^2 + h_A\delta(t). \quad (10)$$

If the traps are donors $n \approx N_d + (N_T - n_T)$. An equation similar to Eq. (10) is obtained by substituting $N_d + N_T$ for N_d. Finally, if we consider the dopant atoms as donor traps themselves then $n \approx N_d - n_d$ and again an equation similar to Eq. (10) is obtained by making the substitution $N_T = N_d$.

So, regardless of the kind of traps, the differential equation that is obtained is of the form

$$\frac{dn}{dt} = A - Bn - Cn^2 + h_A\delta(t). \quad (11)$$

For the three cases considered above the coefficients A, B, and C are given in Table 1.

The differential equation above has been solved in the past using two approximations: operation at room temperature [22] or at very low temperature [26]. To extend the analysis over a wider temperature range we derived in Appendix A the solution to Eq. (11) for any condition. The result obtained in Eq. (A.9) applied to the present situation of small perturbations from the equilibrium condition leads to

$$n(t) \approx \frac{-B+\sqrt{B^2+4AC}}{2C} + h_A \times \exp(-(\sqrt{B^2+4AC})t)1(t). \quad (12)$$

The equilibrium condition and the recovery time constant of the above function, $\tau = 1/\sqrt{B^2+4AC}$, are given in Table 2 for different kinds of traps. We can see that for deep acceptors and donors, the time constants are very small compared with those given in the depletion region. At very low temperatures the recovery from the trapping into dopants is governed by a time constant that increases as the temperature decreases.

From Eq. (12), in analogy with the considerations that led to Eq. (9), we have

$$\overline{\Delta n^2(\omega)} = \frac{\tau_c^2}{1+(\omega\tau_c)^2}\overline{h_n^2(\omega)} \quad \tau_c = \frac{1}{\sqrt{B^2+4AC}}. \quad (13)$$

The noise shape is similar to the one obtained in Eq. (9), except that the time constant is different.

Table 1
Coefficients for the differential Eq. (11) for the 3 cases: acceptors, donors and n-donor doping centers

Trap type	A	B	C
Acceptor centers	$c_n n_1 N_d$	$c_n(N_T - N_d + n_1)$	c_n
Donor centers	$c_n n_1(N_T + N_d)$	$c_n(n_1 - N_d)$	c_n
Dopants	$c_n n_1 N_d$	$c_n n_1$	c_n

Table 2
Stationary condition and recovery time constant for Eq. (12) for different trapping types in a forward biased pn junction

Trap type	$\tau = 1/\sqrt{B^2+4AC}$	$n(\infty)$
Acceptor centers	$\approx 1/c_n(N_d + N_T + n_1)$	$N_d - N_T$
Donor centers	$\approx 1/c_n(N_d + 2N_T + n_1)$	N_d
Donor dopants	$1/c_n(2n_0 + n_1)$	$T = 300$ K: $N_d - n_{d_0}$
	$T \to 0$ K : $\approx 1/c_n n_0$	$T \to 0$ K: n_0

2.3. Counting statistics

Eqs. (9) and (13), having similar shape, give the fluctuation that we expect in the charge carrier population as a response to a random perturbation $\overline{h_n^2(\omega)}$, having a monolateral white frequency spectrum $\overline{h_N^2}$. Integrating either Eq. (9) or Eq. (13) with respect to frequency allows to express $\overline{h_N^2}$ in term of the (for the moment) unknown Root Mean Square (RMS) fluctuation of n, $\Delta n^2_{RMS}(\omega)$:

$$\overline{\Delta n^2(\omega)} = 4\frac{\tau}{1+(\omega\tau)^2}\Delta n^2_{RMS}. \tag{14}$$

For the statistical mathematical evaluation, we need to consider dimensionless quantities. We therefore consider the fluctuation of the total number of carriers contained within a volume V, $n_{Tv} = n_T V$, $N_{Tv} = N_T V$, etc. V may of course depend on position within the semiconductor.

Different approaches of varying accuracy exist for the evaluation of Δn^2_{RMS} [20,27–30]. One of these [31] is based on the classical Stirling formula and Lagrange multipliers, from which the classical Fermi distribution function is obtained. With well-defined available states and a constant total energy it is possible to determine the more probable equilibrium condition. The fluctuation in the charge carrier population is known to be inversely proportional to the sum of the inverse of all the statistical RMS fluctuations. For the case of a two-level system formed by the conduction band and one kind of trapping center we have

$$\begin{aligned}\frac{1}{\Delta n^2_{RMSv}} &= \frac{1}{\sigma_n^2}+\frac{1}{\sigma_{nT}^2}\\ &= \frac{1}{n_{0v}}+\frac{1}{N_{cv}-n_{0v}}+\frac{1}{n_{T0v}}+\frac{1}{N_{Tv}-n_{T0v}}\\ &\approx \frac{1}{n_{0v}}+\frac{1}{n_{T0v}}+\frac{1}{N_{Tv}-n_{T0v}}.\end{aligned} \tag{15}$$

In the above equation, the σ's have been derived from the Poisson statistic. The term that contains N_{cv} has been ignored in the last result above since the doping concentration in the JFET channels is always much smaller than the concentration of the available states in the conduction band.

When we consider a reverse junction, any charge created in the conduction band is swept away in a very short time, and n_{0v} does not fluctuate and can be neglected in Eq. (15). Δn^2_{RMSv} is contributed only by the variance of n_{Tv}. In an n-region, or in a forward biased pn junction away from the transition region, the variance is dependent only on the trapping center concentration N_T any time this concentration is much smaller than the doping concentration, $N_T \ll N_d$, N_c, which is the typical situation, opposed to the one just described. For both these cases we, therefore, have the same mathematical representation:

$$\Delta n^2_{RMSv} = \frac{n_{T0v}(N_{Tv}-n_{T0v})}{N_{Tv}}. \tag{16}$$

The last case we consider is the one in which the noise comes from the dopants themselves, acting as traps. For this case we substitute $N_T = N_d$ and obtain

$$\begin{aligned}\frac{1}{\Delta n^2_{RMSv}} &= \frac{2}{n_{0v}}+\frac{1}{N_{dv}-n_{0v}} \text{ or}\\ \Delta n^2_{RMSv} &= \frac{n_{0v}(N_{dv}-n_{0v})}{2N_{dv}-n_{0v}}.\end{aligned} \tag{17}$$

Let us introduce the Fermi–Dirac function:

$$f_T = \frac{1}{1+\exp[(E_T-E_F)/K_B T]} \tag{18}$$

where E_F is the quasi-Fermi level, which depends on position, bias, and charge type within the semiconductor. K_B is the Boltzmann constant and T the absolute temperature.

In term of f_T the electron concentrations can be expressed by

$$\begin{aligned}n_{T_0} &= f_T\frac{g_T}{1+(g_T-1)f_T}N_T\\ N_T - n_{T_0} &= (1-f_T)\frac{1}{1+(g_T-1)f_T}N_T\end{aligned} \tag{19}$$

where g_T is the degeneracy factor for the electrons at the energy level E_T. Therefore,

$$\begin{aligned}\Delta n^2_{RMSv} &= f_T(1-f_T)\frac{g_T}{[1+(g_T-1)f_T]^2}N_{Tv},\\ &\quad \text{Depleted region, or } n \gg N_T,\\ \Delta n^2_{RMSv} &= f_d(1-f_d)\\ &\quad \times\frac{g_d}{[1-f_d+2g_d f_d][1+(g_d-1)f_d]}N_{dv},\\ &\quad \text{Dopant trapping center effect.}\end{aligned} \tag{20}$$

In addition to the obtained results above, it has to be considered that $\Delta n^2_{\mathrm{RMSv}} = \Delta n^2_{\mathrm{RMS}} V^2$.

From Eq. (20) we can see that the noise is proportional to the product $f_{\mathrm{T}}(1-f_{\mathrm{T}})$ which is a measure of how full a trapping level is. The equation's result says that a trapping level too full or too empty generates a negligible amount of noise. The maximum noise occurs when the trapping level is half full. At room temperature and higher the capturing process competes with the emission process; both have a similar probability of occurring only for the deeper traps located close to the middle of the band gap. The shallow trapping centers, close to the conduction band energy, always have enough thermal energy to jump to the conduction band: they are therefore empty at all times and do not contribute to the G–R noise. As soon as the temperature lowers the shallow levels are more likely to be filled, while the deeper centers become filled most of the time. Consequently, the more effective centers for noise generation become the ones with energy closer to the conduction band. An equivalent consideration can be made for the trapping center near the valence band. A scan in temperature is therefore a useful way to study the presence and the effect of the trapping centers within the band gap.

2.4. G–R equivalent input noise in JFET

2.4.1. Gate noise due to G–R centers present in the depletion region

Let us now calculate the input-referred noise of a JFET due to the mechanisms described in the previous sections. We will start by calculating the noise generated in the depletion region of the JFET. Its effect can be regarded as a change in the gate voltage that arises from the fluctuation of the charge distribution present in the transition region. Given that only one kind of donor trap is present, the one-dimensional Poisson equation within the depletion region is

$$\frac{\mathrm{d}E}{\mathrm{d}x} = \frac{e}{\varepsilon}[n_{\mathrm{n}_0} + (N_{\mathrm{T}} - n_{\mathrm{T}})] \Rightarrow$$
$$E(x) = \frac{e}{\varepsilon}[n_{\mathrm{n}_0} + (N_{\mathrm{T}} - n_{\mathrm{T}})](x - W) \qquad (21)$$

where $E(x)$ is the electric field, negligible at the borderlines of the depletion region, and x has its origin at the gate, according to Fig. 3, ε is the dielectric constant of Si, and W, position dependant, is the width of the depletion region. The positive concentration of ionized atoms is n_{n_0}, which is equal to N_{d} at room temperatures. Let us consider the depletion region to be divided into sheets having thickness $\mathrm{d}x$ and volume $LZ\mathrm{d}x$, where L is the gate length and Z the gate width. The voltage drop across any sheet is $\mathrm{d}v = -E(x)\,\mathrm{d}x$. This voltage may fluctuate due to random fluctuations of n_{T}. Its variance $\delta v^2_{\mathrm{ndr}} = \overline{\mathrm{d}v^2} - \overline{\mathrm{d}v}^2$, according to Eq. (21), and integrated above the whole gate area gives an estimation of the gate noise, once the complex dependences on position within the depletion region of τ and f_{T} are known. To simplify calculation one can consider a first approximated solution valid only for shallow levels, at low temperatures [32,33], for which f_{T} and τ are considered constant and different from zero only in a limited portion ΔW_{T} of the channel. Alternatively, for depth traps τ and f_{T} can be considered constant across the whole depletion region [22–24], since in this case the chance for an electron to be emitted from a trap center shows a small sensitivity to the applied bias voltage. As a

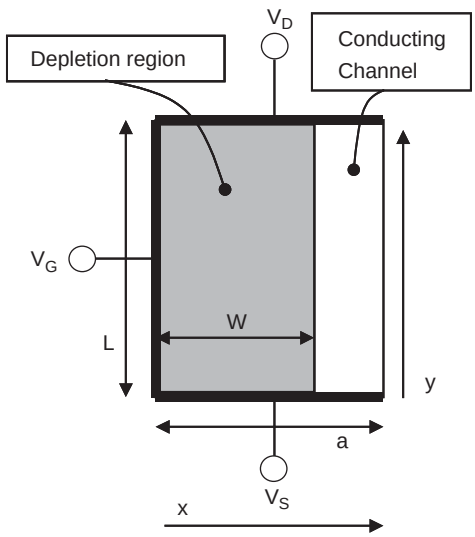

Fig. 3. One-dimensional model of a JFET in the saturation region. The width Z of the transistor is orthogonal to the paper.

consequence, a finite population of electrons must occupy levels at the trap energy E_T within the depletion region; hence the energy difference between E_T and the quasi-Fermi level must remain constant in the depletion region, to allow the Fermi function f_T to account for the finite population of trapped electrons. This is particularly true at large reverse bias, where this concept also becomes valid for more shallow levels. Because in this case both n_0 and p_0 are negligible, Eqs. (8)and (19) results in

$$f_T \frac{g_T}{1+(g_T-1)f_T} = \frac{c_n n_0 + c_p p_1}{c_n(n_0+n_1)+c_p(p_1+p_0)}. \quad (22)$$

If both n_0 and p_0 are much smaller than n_1 and p_1 in the major part of the depletion region, f_T becomes constant within the reverse region since n_1 and p_1 do not depend on bias (Eq. (5)):

$$n_1 = N_C \exp\left(\frac{E_T - E_C}{K_B T}\right),$$
$$p_1 = N_V \exp\left(\frac{E_V - E_T}{K_B T}\right). \quad (23)$$

To address the problem that the two above approximations are not able to fit data for any kind of traps, we have introduced a new approach. Let us perform the integration of Eq. (21) above the whole depletion region $(0, W)$, and also use the theorem of the weighted average for integrals $(\int_a^b f(x)g(x)\,dx = f(c)\int_a^b g(x)\,dx$ with $c \in (a,b))$. By defining $f(x) = f_T(1-f_T)\tau/[1+(g_T-1)f_T]^2/[1+(\omega\tau)^2]$, $g(x) = (x-W)^2$ and using the results of Appendix B, we get

$$\overline{v_{gndr}^2} = \frac{f_{TC}(1-f_{TC})g_T}{[1+(g_T-1)f_{TC}]^2}\frac{N_T}{n_{no}}\frac{8}{3}\frac{eV_P}{C_G}\frac{\tau_C}{1+(\omega\tau_C)^2} \times \left[1-\frac{I_{DS}}{2V_P g_m}\right]^3,$$
$$c \in (0,W), \quad C_G = \frac{\varepsilon LZ}{a}. \quad (24)$$

This equation does not provide much data from a mathematical point of view, since for its evaluation we must know the point c within $(0, W)$ where the necessary quantities must be calculated. Nevertheless, it is very useful from an experimental point of view. From Eq. (22) we see that for every kind of trap (shallow or deep) with an energy level smaller than the dopant energy level, there exists a temperature and a position starting from the channel side of the depletion region, at $x = W$, going toward the gate side of the depletion region, at $x = 0$, where n_0 takes a value that allows f_{TC} to be equal to 0.5. This is evident if we consider that at $x = W$, n_0 is of the order of $N_d > n_1$ for temperatures lower than the temperature at which the Fermi level within the channel is larger than E_T, and at $x = 0$ n_0 is negligible, or

$$\frac{n_0}{n_1} = \exp\left(\frac{E_F - E_T}{K_B T}\right). \quad (25)$$

At the position and temperature at which E_F equals E_T the value of f_{TC} approaches its maximum, resulting in following situation (p_0, $p_1 \approx 0$):

$$f_{TC}(1-f_{TC}) \approx \frac{(c_n n_{oC})(c_n n_1)}{[c_n n_{oC} + c_n n_1]^2} \approx \frac{1}{4} \quad \tau_C \approx \frac{1}{2c_n n_1}. \quad (26)$$

A similar expression can be derived if $p_1 > n_1$.

In a temperature interval approaching its maximum value, f_{TC} has a very small dependence on temperature and on the time constant τ_C. A very robust way to investigate this condition is to plot Eq. (24) with respect to the time constant τ_C, at different temperatures, for frequencies ω such that $\omega\tau_C \ll 1$. If the noise is found to be linearly dependent on τ_C, this indicates that the Fermi function is close to 0.5, which is an indirect confirmation that the G–R noise we are investigating is produced by a single G–R process. Also, from Eq. (24) it is possible to extract information about the concentration of the trapping centers, once the other measurable parameters are known.

If the traps responsible for the noise under investigation are the conductivity dopants, the condition of Eq. (26) has a very small probability to be satisfied at very low temperature (see Eq. (25) when $E_T = E_d$). Hence f_{TC} for dopants can be considered negligible, like also the generated noise in the depletion region, for most of the temperatures of interest.

Eq. (24) is valid only in the saturation region of transistor operation. The extension of its validity to the linear region is not considered here. In first approximation it can be derived by substituting V_{DS} with $|V_{GS}|$.

2.4.2. Gate noise due to G–R center present in the channel region

In the channel region the noise is due to the fluctuation of the charge carriers in the conduction band. For this case the quasi-Fermi level is constant in the channel and coincides with the Fermi level because the bias does not change the energy profile: the current in the channel is due only to drift. This consideration is described by the following expression:

$$\frac{\overline{\Delta I_D^2}}{I_D^2} = \frac{\overline{\Delta n_v^2}}{n_v^2} \tag{27}$$

which is equivalent to a voltage noise at the gate of

$$\overline{v_{nch}^2} = \left(\frac{I_D}{g_m}\right)^2 \frac{\overline{\Delta n_v^2}}{n_v^2}. \tag{28}$$

As will be evident below, the traps in the channel have negligible effect compared to the corresponding traps in the depletion region, except for the very shallow ones at very low temperatures. We, therefore, concentrate only on the noise that originate from the donor levels. Using Eq. (20) and the definitions of Appendix B we get, after a few calculations, the following expression valid for dopant traps (an equivalent equation can be easily derived for a generic trap level):

$$\overline{v_{nch}^2} = 4e\frac{V_{GS}-V_T}{C_G}\frac{g_d f_d^2}{[1-f_d+2g_d f_d][1-f_d^2]} \times \frac{1}{c_n N_d}\frac{1}{1+(\omega\tau_c)^2} \tag{29}$$

where we have considered that

$$\tau_c = \frac{1}{c_n(n_1+2n_0)} = \frac{f_d}{c_n N_d(1-f_d^2)}. \tag{30}$$

The last term of Eq. (29) can be approximated to one in almost all our measurements since the Lorentzian frequency corner is much larger than the instrumentation bandwidth limit (52 KHz). This noise looks like white noise in a wide temperature range even though the mechanism responsible for it is the G–R noise from dopants. The channel noise characterization is therefore a measure of the Fermi function.

Even for this case the expression for the gate voltage depends on the working point. Its contribution is minimal when the conducting channel is thin, at small drain current, or when V_{GS} is close to V_T.

It must be pointed out that the total input noise is the sum of the two calculated contributions, the one coming from the depletion region and the one coming from the channel region ($\overline{v_{ntot}^2} = \overline{v_{ndr}^2} + \overline{v_{nch}^2}$). Nevertheless, since at every selected temperature only a restricted species of traps contribute to the G–R noise, in the above equation it is almost always verified that only one of the two mechanisms dominates. For instance, for a deep or shallow trap in the depletion region at the temperature where it shows its maximum effect, the resulting Lorentzian time constant is much larger than the one generated by the corresponding trap located in the channel region. From Table 2 and Eq. (6), with n_0 negligible in the depletion region, the ratio of the Lorentzian time constants of the channel and of the depletion region due to a donor trap is proportional to n_1/N_d. This ratio is negligible as long as $N_d \gg n_1$, which happens for deep level traps. The two time constants should approach each other for shallow traps, or when N_d approaches n_1, a condition accomplished at very low temperatures. Nevertheless, Eq. (26) is not satisfied at very low temperature and τ_C is very large since hole generation is a very rare process for shallow donors (electron capture from the conduction band is highly inhibited in the depletion region). The effect stems from the fact that the Fermi level in the depletion region is close to the trap energy level when the maximum noise effect is measured, while it is close to the dopant's energy level in the channel. This evaluation applies also to the study of G–R noise generated by the dopants themselves. In this case the dopant levels inside the depletion region are empty down to very low temperatures, where the freeze-out occurs, since the generation of holes from that energy level is very difficult. The term $f_{TC}(1-f_{TC})$, evaluated in the depletion region, is therefore negligible in comparison to the competitive term inside the channel region.

3. The measurement apparatus

3.1. The environment for room temperature characterization

JFET processes optimized for room temperature operation have been measured from -60°C to

+70°C. This temperature range was found adequate for the study of the deep level traps responsible for the LF region of the noise spectra. A temperature chamber, VT7004 by Vötsch, was used for controlling the temperature of the DUT. Measurements have been made simply by putting the whole preamplifier inside a metallic box shielded with a sheet 0.1 mm thick of SKUDOTECH® [35], a special metal alloy designed for having strong magnetic field rejecting properties. Shielding was necessary to avoid the interference coming from the fan coil present inside the temperature chamber.

3.2. The cryogenic setup

The cryogenic measurement setup has been especially designed to eliminate microphonics at low frequencies. For this reason the measurement system was designed without using mechanical pumps for cooling, stabilizing temperature, or maintaining a vacuum environment around the DUT.

The DUT is put at one end of a stainless steel tube of 10 mm diameter. Inside the tube are wires that connect the DUT and diagnostics to the room temperature second stage located at the other end of the tube. The DUT is surrounded by an aluminum cylinder, which is screwed on a stopper located a few cm above the DUT. Fig. 4 shows a picture of the setup.

The DUT is brought to a stable low temperature position by inserting the apparatus in a dewar half filled with LN2 or LHe. The temperature is set by adjusting the distance from the DUT to the cold liquid surface inside the dewar. In this arrangement, the DUT is surrounded by a metal surface with a slightly lower temperature. This creates a cryo-pumping effect: the condensable components of the air inside the cylinder condense on the wall of the cylinder instead of on the DUT. Consequently, ice cannot form on the DUT, and it is not necessary to create a vacuum inside the cylinder. Thus, no pumps are necessary to make and/or maintain a vacuum. This principle of operation is opposite to that of any standard cryogenic system. In those instruments the DUT is the coldest part of the system, so a vacuum is required for preventing any condensation of the gas on it.

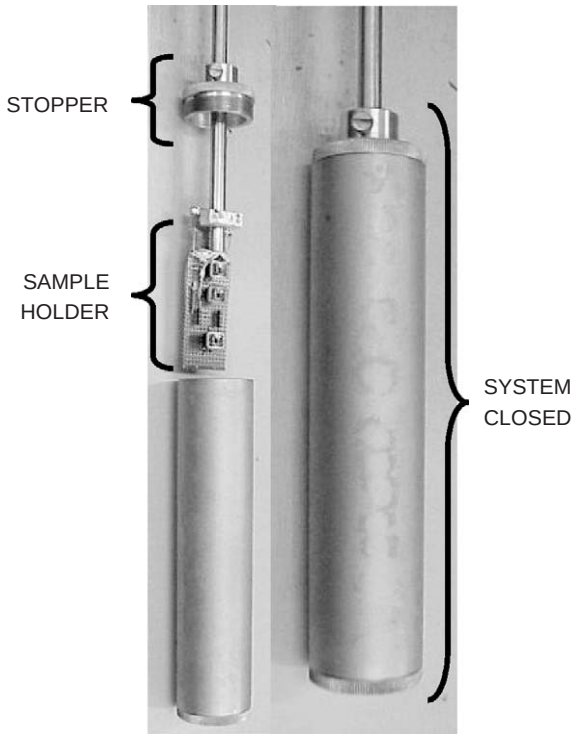

Fig. 4. Photograph of the cryogenic setup implemented for minimizing microphonic effects.

The presence of ice must be avoided since it can deteriorate the noise performances. At LF, when measuring parallel noise or leakage currents, the presence of ice can add even more disturbances. On the other hand the absence of any pump or compressor for creating and maintaining the cryogenic temperature is by far the more important benefit to the LF noise measurements, as in this case microphonics and electromagnetic interferences induced by the vibration coming from motors motion is avoided.

Since the power dissipated by the DUT and its associated bias circuitry is small ($\sim$10 mW) this temperature setting procedure has been shown to be very stable. Stability within a few tens of mK are readily obtained over periods of about one hour. Over time intervals required for a measurement (typically 15 min) no significant temperature variation has been observed, as long as the dewar was not too empty or too full.

3.3. The measurement configuration

Characterizations of transistors have been made using two different set-ups. In the first case JFETs were characterized in a temperature range around room temperature. The pair of selected JFETs DUT formed the differential input stage of the amplifier APRE in the schematic diagram of Fig. 5. This amplifier is similar to the one described in Ref. [36]. The amplifier gain has a low frequency cutoff whose -3 dB is 0.5 Hz. The flat band voltage gain is 1000 V/V. The amplifier output is further increased by a factor of 10 by the additional stage AEND. The contribution to the input noise of APRE coming from the circuit elements that follow the JFETs pair in APRE has been found negligible. The feedback contributes to the series noise mainly due to the thermal noise of the 33 Ω resistor, $0.74\,\mathrm{nV}/\sqrt{\mathrm{Hz}}$ at 300 K. This can be subtracted out of the experimental measurements.

In the second case, as shown in Fig. 6, the signal of the JFET DUT held at cryogenic temperature is fed into APRE, now used as the second stage of amplification. The only contribution to the noise coming from APRE is in this case its series noise that, due to the configuration adopted, can be measured in a very accurate way and can be removed from the overall noise measured. The DUT located at cryogenic temperature is biased in the simplest possible way: common drain configuration, Fig. 6. This configuration has many benefits. It is self-biased, so it is not necessary to adjust the electrical parameters when the temperature changes. The gain from the input gate and the source, at its output, is closed to one. Calibration of the gain is made by injecting a signal at the input gate. The transfer function obtained in this way is the same as that of the series gate noise. Once the transfer function has been measured, the input gate of the DUT is connected to ground with the 50 Ω resistor R_{IN}, minimizing pick-up noise. The source of the cold JFET under test is readout by APRE, with a link length of about 1 m. Since the source of the DUT is a low impedance node, microphonism is minimized. The biasing resistor at the DUT source, R_S, is held at cryogenic temperature, close to the DUT, to make its thermal noise contribution negligible.

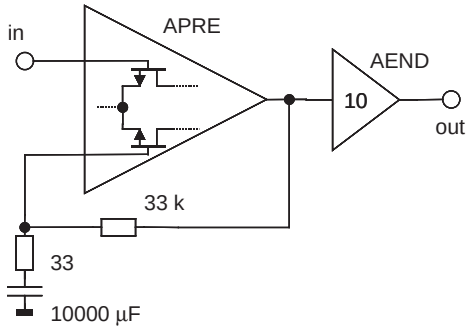

Fig. 5. Schematic diagram of the preamplifier used for noise measurements.

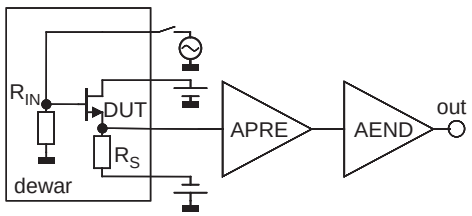

Fig. 6. Schematic diagram of the cold JFET readout.

3.4. Measurement procedure

For both kinds of configuration, an HP35670A spectrum analyzer was used to read the output of the system. For each temperature setting the procedure starts with the measurement of the transfer function that is obtained by the ratio between the output voltage of the system and the injected input signal, white noise. The second step consists of removing the input signal and measuring the system noise. The floor noise of the apparatus is then subtracted from this measurement. For room temperature JFET characterization the floor noise consists of the thermal noise of the feedback resistors. For cold temperature JFET characterization the floor noise is that of the whole APRE. For both cases the result is divided by the transfer function, to refer the noise to the input. The noise has been measured in the frequency span 1 Hz–52 KHz, and it is represented in a log-log scale. The HP35670A measures the power spectrum using the Fast Fourier Transform, which is an algorithm that operates in the linear scale time-frequency. To obtain accurate analysis, it is

necessary to have the same number of points per decade in frequency. To this aim we have performed one measurement for every frequency decade, and then concatenated the data. So each noise spectrum consists actually of 5 measurements: the first with the instrument bandwidth limited to 10 Hz, the second to 100 Hz, the third to 1 KHz, the fourth to 10 KHz and the last to the full span of 52 KHz. The same steps are performed with the measurement of the transfer function. In this way a very precise representation of the noise is obtained in the whole range of frequency investigated, easily allowing the study of the trap behavior with temperature.

The described approach of measuring the noise spectra versus temperature [37–39], is different from that used in many previous experiments [34,40–45]. In those cases G–R noise was extracted from noise measurements realized in a narrow frequency span around a chosen measurement frequency, ω_M, looking for a maximum with temperature. This approach has been found to be inaccurate at low temperature. Following this procedure the shape around the maximum of the noise of Eq. (24), as a function of temperature, is considered to be dominated mainly by the term $\tau_C/(1+(\omega_M\tau_C)^2)$. As a result, a maximum should be obtained when the measurement frequency, ω_M, equals the Lorentzian frequency $1/\tau_C$. Actually, in Eq. (24), the maximum should instead considered proportional to $f_{TC}(1-f_{TC})\tau_C/(1+(\omega_M\tau_C)^2)$, a more complicated function of temperature, that does not necessary have a peak at $\omega_M = 1/\tau_C$.

We measured the noise spectrum at a selected temperature, finding the Lorentzian frequency $1/\tau_C$ from the roll off of the spectrum. This measurement is independent of the noise amplitude, hence also independent of $f_{TC}(1-f_{TC})$. In addition, the value of the flat part of the Lorentzian component of the noise, we can now discuss, is proportional to the product $f_{TC}(1-f_{TC})\tau_C$ (see Section 2.4.1). After making a temperature scan, we added a further analytical step by plotting the noise amplitudes of the Lorentzian components as a function of the Lorentzian frequencies. For a robust description of the noise, we look for the region where this curve is linearly dependent on τ_C. This condition is fulfilled close to the maximum of the function $f_{TC}(1-f_{TC})$, where the temperature dependence of this term shows its minimum sensitivity. Therefore, our approach allows us an additional degree of freedom. The two interesting parameters to be extracted are the trap cross-section, which is proportional to the Lorentzian frequency, and the trap density, which is proportional to amplitude of the Lorentzian noise contribution. In our procedure these two quantities become now two measurement parameters.

4. The effects of deep level traps on the noise

The noise is dependent on the quasi-Fermi level. In this case the dominant noise source is localized in the depletion region (see Eq. (24)) and the largest contribution to the noise is from those traps with an energy level close to the quasi-Fermi level, for which $f_{TC}(1-f_{TC})\approx 0.25$. At room temperature this happens for traps with activation energy close to the middle of the band-gap. To study the effect of G–R noise around room temperature we have selected two very low noise JFET processes: the dual 2SK146 from Toshiba and the dual SNJ3600 from Interfet. We have measured their noise in the temperature range -60°C to 70°C using the set up described in Section 3.1. Each of the JFETs of a pair were connected as the input device of the preamplifier of Fig. 5. The whole preamplifier was then put inside the temperature chamber. The temperature was stepped by about 10°C between the indicated limits. In Fig. 7 the series noise over the full temperature range for each of the dual 2SK146 JFETs is shown in a 3D-plot, after the noise of the feedback resistor has been subtracted. Each JFET was operated at $I_{DS} = 1$ mA and $V_{DS} = 1$ V. The presence of a trap is evident whose G–R noise starts from about -40°C. As the temperature increases the noise due to this trap decreases, while the frequency of the G–R process increases. At the larger temperatures the amplitude of this G–R noise disappears and the LF noise starts to increases again, probably due to the presence of another kind of trap. In Fig. 7 a mathematical fit to each noise spectrum is superimposed. To fit

data we chose a simple function that showed the effect of a single trap, using only a few parameters:

$$\overline{e_j^2} = \frac{A_f}{f^{esp}} + \frac{A_{LOR}}{1+(f/f_{LOR})^2} + \overline{e_{white}^2}. \quad (31)$$

The first term above accounts for possible presence of traps at very small frequencies. The second term describes a trap having an amplitude A_{LOR} and time constant $1/(2\pi f_{LOR})$. The last term is the white noise.

As shown in Fig. 7 the above interpolating function satisfactory accounts for the measured noise. To fit the spectra we have used the χ^2 technique with the robust estimator [46], which allows weighting the data to be interpolated with terms proportional to a power of the inverse of the value of the data itself. This fitting algorithm was applied to the noise power measured, although in the following figures only the square root of the noise will be shown. The same procedure has been adopted for the SNJ3600, operated at 5 mA of drain current and 1 V of V_{DS}. The noise versus temperature plots obtained for it, together to the fit results, are shown in Fig. 8.

From the parameters extracted by the fittings a number of facts can be deduced. Let us start by examining the frequency behavior of the Lorentzian traps. The associated time constant is given in Eq. (8). If we assume that we are close to the maximum for the product $f_{TC}(1-f_{TC})$ then

$$\tau \approx \frac{1}{2c_n n_1} \quad \text{or} \quad \frac{1}{2c_p p_1}. \quad (32)$$

Therefore, if $n_1 \gg p_1$:

$$\frac{1}{\tau} \approx 2c_n n_1 \approx 4\left[\frac{2\pi K_B m_n}{h^2}\right]^{3/2}\left[\frac{3K_B}{m_n}\right]^{1/2} \times \sigma T^2 \exp\left(\frac{E_T - E_C}{K_B T}\right). \quad (33)$$

On the other hand, when $p_1 \gg n_1$ we obtain:

$$\frac{1}{\tau} \approx 2c_p p_1 \approx 4\left[\frac{2\pi K_B m_h}{h^2}\right]^{3/2}\left[\frac{3K_B}{m_h}\right]^{1/2} \times \sigma T^2 \exp\left(\frac{E_V - E_T}{K_B T}\right) \quad (34)$$

where σ is the capture cross-section from the trap, m_n and m_h the reduced mass for electrons and holes, respectively, and h the Plank constant.

We expect the Lorentzian frequencies to be proportional to the product of the square of the temperature and to the exponential of the ratio of the energy of the trap, measured with respect to the appropriate band level and divided by the

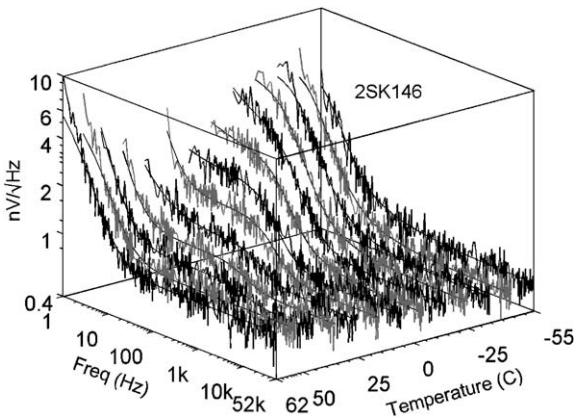

Fig. 7. 3D-plot of the noise spectra measured for the JFET 2SK146. To each noise spectrum the calculated fit is superimposed.

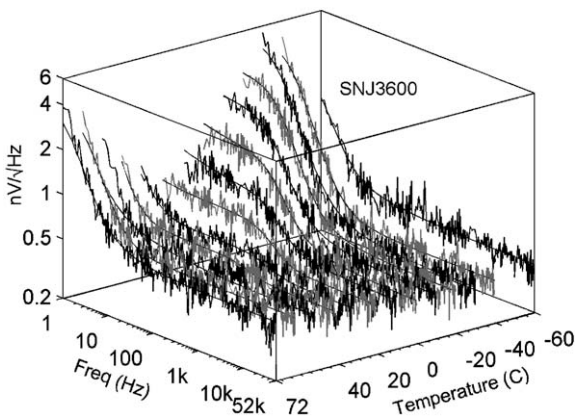

Fig. 8. 3D-plot of the noise spectra measured for the JFET SNJ3600. To each noise spectrum the calculated fit is superimposed.

temperature. From this kind of measurement it is not possible to determine if the trap is a donor or an acceptor since for both cases the trap energy is measured with respect to the conduction band or the valence band, respectively, with the same final effect on the shape of the function.

The temperature dependence of the Lorentzian frequencies, f_{LOR}, with respect to the inverse of temperature is shown in the log–log plot of Fig. 9 for both the JFETs. It is very interesting to observe that, although the JFET were manufactured with different processes and by different companies, the temperature dependence of the G–R noise due to the observed traps in this temperature range is exactly the same. If we discard the Lorentzian frequencies obtained by fitting the data at lower and higher temperatures, whose values are at the limits of sensitivity, all the parameters can be fitted by a single function that can be deduced by the above Eqs. (33) and (34). The fitting function used, that depends on two parameters a and b, has been

$$f_{LOR} = a\frac{1}{x^2}\left(\frac{e}{K_B}\right)^2 \exp(bx)\,(\mathrm{Hz}), \quad x = \frac{e}{K_B T} \tag{35}$$

where e is the electron charge.The fit is plotted in Fig. 9, superimposed to the extracted data. The temperature range over which Eq. (35) is applied is the one where the coefficient A_{LOR} in Eq. (31) is

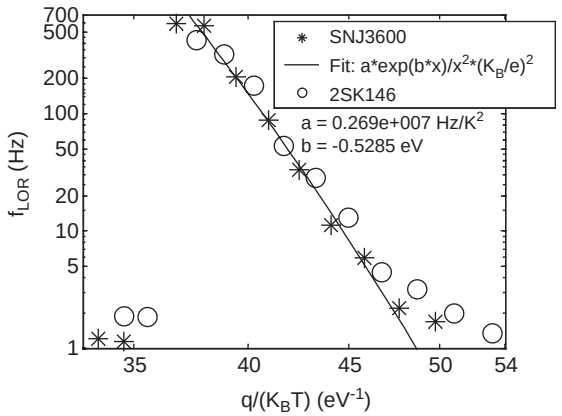

Fig. 9. Log–log plot of the Lorentzian frequencies versus the inverse of the temperature for both the SNJ3600 (∗) and the 2SK146 (○) JFETs.

linearly dependant on $1/(2\pi f_{LOR})$. From Eq. (24) it is seen that this property is satisfied by a Fermi-function which is flat in the considered temperature range, allowing us to get a better approximation of f_{LOR} that, in turn, depends in some way on the Fermi-function itself. As can be seen, the energy of the trap (fitting parameter b) is located about 0.50 eV above the valence band or below the conduction band. This energy is typically attributed to gold acceptors. From the fitting parameter a it is possible to extract the order of magnitude of the cross-section σ, from the Eqs. (33)–(35):

$$\sigma = a\frac{m_e}{m_{n(h)}} 9.65 \times 10^{-22}\ \mathrm{cm}^2. \tag{36}$$

For the case in which the electron reduced mass is close to $0.5\,m_e$, σ results about $10^{-14}\,\mathrm{cm}^2$, using the fitting parameter a from Fig. 9. For holes, which have reduced mass of about $2\,m_e$, the cross-section is about $10^{-15}\,\mathrm{cm}^2$. This is consistent with the values obtained by other studies [22], [47].

We can also attempt to deduce the concentration of the traps responsible for this G–R noise. Because of the expression for the G–R noise given in Eq. (24), we can estimate the concentration of the trap as a function of only measured parameters and on the channel doping profile. In Eq. (24) the only parameter that it is difficult to know in the depletion region is the Fermi function. Let us suppose in advance that it is quite constant and equal to 0.5 in the temperature range considered. If this were true, as described above, we would expect the amplitude of the Lorentzian noise to be linearly dependant on the Lorentzian time constant τ_C. In Fig. 10 the plot of the coefficients of the Lorentzian amplitudes, A_{LOR}, versus the inverse of Lorentzian frequencies are plotted for the 2SK146 (and the SNJ3600), after the parameters extracted at the lower and higher temperatures have been excluded. From the figure it is possible to see that the behavior is almost linear, and, therefore, the Fermi function can be assumed to be almost constant. From Eqs. (31) and (24) we can approximate

$$A_{LOR} \approx \frac{N_T}{n_{n_0}}\frac{V_P}{C_G} 1.3 \times 10^{-20}\frac{1}{f_{LOR}} V^2/\mathrm{Hz}. \tag{37}$$

The coefficient indicated in the above equation is the mean value between the results from setting the degeneracy factor g_T equal to 2 (donor traps) and setting g_T equal to 4 (acceptor traps). The ratio for the two cases is about 40%.

For the 2SK146 V_P is about 1.1 V and the input capacitance (for the fully depleted condition) is close to 65 pF [48]. Using Eq. (37) and the slope extracted from Fig. 10 we calculate that the ratio N_T/n_{n_0} is about 4×10^{-7}. If we consider that the typical doping concentration for a JFET channel is of the order of 10^{16} atoms/cm^3, we can estimate the concentration of the G–R traps at 0.50 eV in the 2SK146 to be about 4×10^9 atoms/cm^3.

The same estimation has been made also for the SNJ3600 (see again the fit of Fig. 10). This device has V_P of about 2 V and an input capacitance of about 500 pF [48]. Consequently the ratio N_T/n_{n_0} has the order of magnitude of about 10^{-6}, or concentration N_T of about 10^{10} atoms/cm^3 for the case that N_d is of the order of 10^{16} atoms/cm^3.

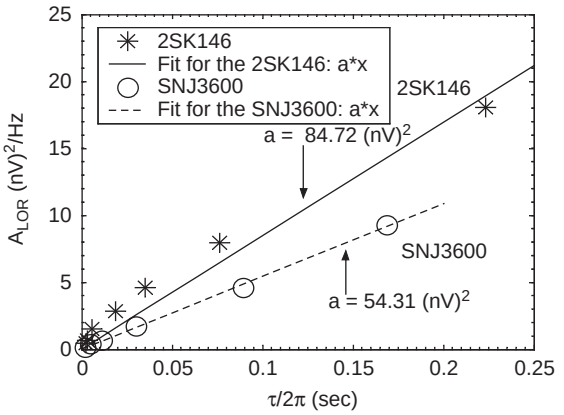

Fig. 10. Amplitude of the Lorentzians with respect to the Lorentzian time constant for the JFET 2SK146 and for the SNJ3600.

In Table 3 the parameters of interest for both the Silicon JFETs 2SK146 and SNJ3600 are summarized.

5. The effects of shallow level traps on the noise

The shallow level traps have the maximum effect on the G–R noise at lower temperatures than the deeper traps. Reducing the temperature reveals their presence. We have selected a very low noise Si JFET process especially designed for low temperature operation [49]. We scanned the temperature in two ranges: from 80 K to about 150 K and from 80 K down to 14 K. In this section, we will shown the results for the first situation. We have measured different JFET transistor types from Moxtek. In Fig. 11 the 3D-plot of the JFET MX16RC noise is shown measured in the temperature range from 95 to 150 K. The presence of a trap is evident through its effect seen in the LF region of the spectra over the temperature range 95–125 K. Another device type for which evidence of a shallow trap is visible is the MX17-OLD shown in Fig. 12. This device has been labeled OLD to distinguish it from another device of the same type received later in our lab. The interesting fact is that for this latter sample it was possible to see the effect due to another kind of trap (Fig. 13). In these three figures the fitting curves have been added, calculated using Eq. (31).

We have also extracted the parameters of interest from the above measurements. In Fig. 14

Table 3
Extracted parameters for the traps responsible of the G–R noise for the 2SK146 and SNJ3600

	V_P/C_G (V/pF)	N_T/N_d	a of Eq. (35) (Hz/K^2)	$\|b\|$ of Eq. (35) (trap energy) (eV)	σ (cm^2)	Trap candidates
2SK146	1.1/65	4×10^{-7}	2.22×10^5	0.53	1×10^{-14}	Mn (0.53), Cd (0.55), Au (0.54 A), Co (0.53A), Cu (0.53), Fe (0.51), O (0.51)
SNJ3600	2/500	1×10^{-6}	5.85×10^6	0.53	1×10^{-14}	

The terms a and b are the parameters extracted from the fitting function given in Eq. (31). In the last column in parenthesis is the energy measured from the nearest band edge. The levels are donors except those indicated with the letter A.

the coefficients A_{LOR} has been plotted as a function of the inverse of the Lorentzian frequencies. As can be seen, over the temperature range considered, a linear fit works well. In Fig. 15 we plotted the Lorentzian frequencies versus the inverse of temperature. The fit has been calculated for the temperature range found in Fig. 14. The summary of the parameters extracted from the measured noise is given in Table 4. These three JFETs have shown a moderately small noise. The concentration of the traps has been found to be small compared to the donor concentration.

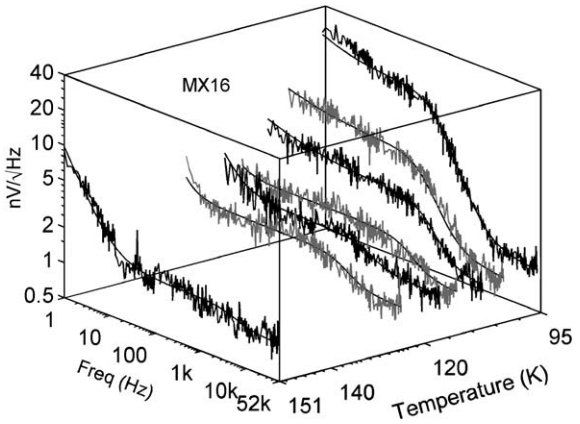

Fig. 11. 3D-plot of the noise spectra measured for the JFET MX16. To each noise spectrum the calculated fit is superimposed.

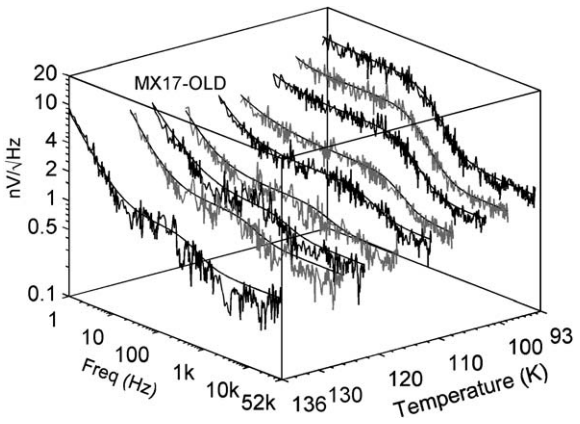

Fig. 12. 3D-plot of the noise spectra measured for the JFET MX17-OLD. To each noise spectrum the calculated fit is superimposed.

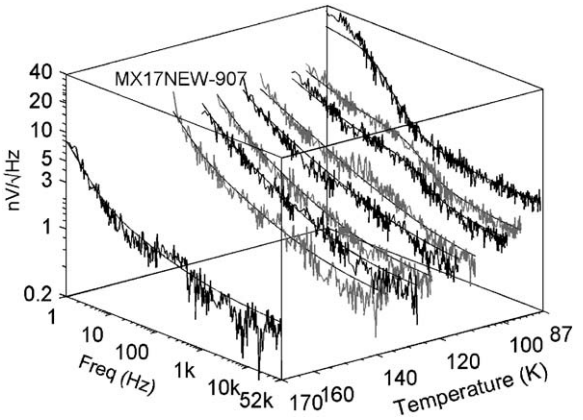

Fig. 13. 3D-plot of the noise spectra measured for the JFET MX17-NEW. To each noise spectrum the calculated fit is superimposed.

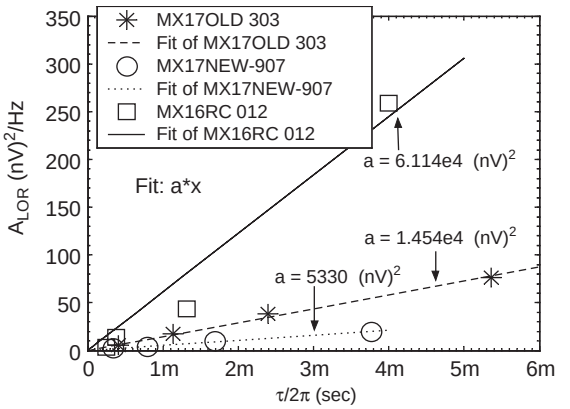

Fig. 14. Coefficients A_{LOR} of Eq. (31) as a function of the Lorentzian frequencies for the 3 JFETs MX16RC, MX17-OLD and MX17-NEW.

The smaller concentration resulted for the MX17-NEW to be about 2×10^{10} atoms/cm^3, once N_d has been assumed to be equal to 10^{16} atoms/cm^3. The cross-section follows the same rule of the previous section, applying Eq. (36). In Table 4 some possible candidates for the found traps are given. As can be seen, around 100 K the difference between the trap energy and the band edge is around 0.1 eV.

Another transistor of this series had even better performances. In Fig. 16 the 3D-plot of the noise of the MX11CD is given for the temperature range

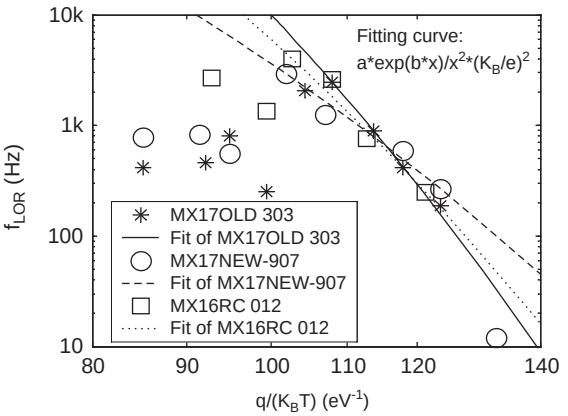

Fig. 15. Lorentzian frequencies for the 3 JFETs MX16RC, MX17-OLD and MX17-NEW and the respective interpolating fits.

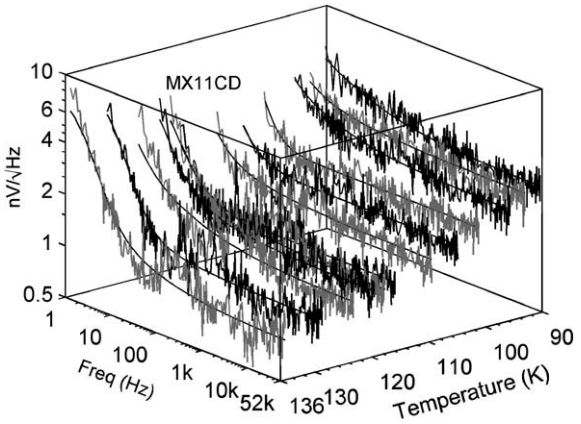

Fig. 16. 3D-plot of the noise spectra measured for the JFET MX11CD. To each noise spectrum the calculated fit is superimposed.

Table 4
Extracted parameters for the traps responsible of the G–R noise of the 3 JFETs MX16RC, MX17-OLD and MX17-NEW

	V_P/C_G (V/pF)	N_T/N_d	a of Eq. (35) (Hz/K^2)	$\|b\|$ of Eq. (35) (trap energy (eV)	σ (cm^2)	Trap candidate
MX16RC	2.5/44	8.3×10^{-5}	2.22×10^{5}	0.1312	4.5×10^{-16}	Mg (0.11 A), Te (0.14), Fe (0.14)
MX17-OLD	4.7/22	5.2×10^{-6}	5.85×10^{6}	0.1587	1.15×10^{-14}	O (0.16), Pb (0.17 A), Be (0.17A)
MX17-NEW	4.7/22	1.9×10^{-6}	2.95×10^{3}	0.09297	5.5×10^{-18}	Ga (0.072 A), Mg (0.11 A)

The terms a and b are the parameters extracted from the fitting function given in Eq. (31). In the last column in parenthesis is the energy measured from the nearest band edge. The levels are donors except those indicated with the letter A.

90–140 K. As can be seen at the optimum temperature of operation for the LF noise, about 110 K, this transistor has a negligible LF noise. For the MX11CD it was not possible to find the presence of any kind of traps in this temperature range. Many other devices of the MX process have shown these very excellent characteristics [50].

Another interesting property of the MX11CD is that its pinch-off voltage is close to 5 V. This feature made this device attractive for testing at much lower temperature, as will be evident later.

6. Electric field effects at low temperatures and operating conditions

In all the previous sections, we have neglected any possible field effect on the energy profile of the electrons inside the samples, although the applied electric field would introduce a small perturbation of the energy profile. Another effect to be considered, as the temperature is lowered, is electron freeze-out, or more accurately, carrier trapping at dopant sites. This effect can limit the performance of the transistor if some technological precautions are not taken [51].

A JFET to be operated at low temperature needs an important requirement to be satisfied. From Eq. (B.7) we see that the maximum current that can flow between drain and source, I_{DSS}, is obtained when $V_{GS} = 0$ V, or

$$I_{DSS} = en_{n_0} Za\mu \frac{V_{DS}}{L}\frac{1}{2}\frac{(-V_T)}{V_P}. \quad (38)$$

From above it is evident that for I_{DSS} to be positive V_T needs to be negative. The threshold

voltage V_T can be deduced from Eq. (B.2), repeated here

$$V_T = V_{bi} - V_P = V_{bi} - \frac{en_{n_0}a^2}{2\varepsilon}. \quad (39)$$

There are two situations to consider. At temperatures above about 70 K the carrier concentration n_{no} can be approximated by the doping concentration N_d in almost all situations encountered with conventional JFETs [52]. The temperature coefficient of V_T therefore coincides with that of V_{bi}, or $-2\,mV/^\circ C$. At temperatures smaller than 70 K, n_{n_0} decreases in value and the temperature coefficient of V_T becomes even more negative, leading V_T to 0 V as the temperature lowers. For instance at 70 K V_{bi} is about 1 V, so we need $V_P \geqslant 1$ V, let us say 1.2 V to have $V_T < 0$. To achieve this at room temperature V_T must be less than -0.6 V. This value for V_T is the maximum threshold voltage that a JFET capable of working at 70 K should have at room temperature. The pinch-off voltage, V_P, should be even larger for the JFET to work at temperatures smaller than 70 K.

As shown in Eq. (39) the designer has two degrees of freedom for increasing the pinch-off voltage V_P: he can increase the doping concentration and/or increase the channel thickness a [51]. The adoption of a large thickness for a is the better choice, since it allows the designer to obtain large values of the transconductance over the input capacitance ratio. This is because g_m is proportional to a, while the input capacitance is inversely proportional to a. In addition, a large thickness allows the designer to employ a small dopant concentration, obtaining a large mobility at low temperatures, since there is lower scattering from the doping atoms [53]. Furthermore, a lower channel doping lowers the gate junction capacitance because the transition from n to p type is less abrupt.

For instance, the MX11CD JFET from Moxtek has a channel thickness of 1.5 μm, from which we can estimate a doping concentration between 2 and 3 times 10^{15} atoms/cm^3, considering a pinch-off voltage V_P between 3 and 5 V at room temperature [53]. The MX11CD has been found to be an excellent candidate for operation down to 14 K.

When an electric field is applied, a force is given to the electrons, even if they are trapped. This force increases their potential energy. Therefore, the energy (principally thermal) needed for the electrons to escape from the trap levels becomes smaller as the electric field is increased. This phenomenon is known as Poole–Frenkel effect [54]. We can approximate the energy profile of a trapped electron with a potential well model. As soon as the electron escapes from the trapping center, it is subject to an attractive force proportional to the square of the inverse of the distance from the well. If a local constant electric field is further applied, the resulting energy profile is the sum of the two effects:

$$U \approx -\frac{e^2}{4\pi\varepsilon r} - eEr. \quad (40)$$

The maximum of U, with respect to the distance r, now bent to negative values far from the barrier, coincides with the barrier lowering and is

$$\Delta U_{PF} \approx -\sqrt{\frac{eE}{\pi\varepsilon}}\ (\text{eV}). \quad (41)$$

In the depletion region the electric field applied between the gate and the channel is proportional to the distance from the gate. Substituting Eq. (21) into Eq. (41) we get:

$$\Delta U_{PF} \approx -\frac{e}{\varepsilon}\sqrt{\frac{n_{n_0}|x - W|}{\pi}}\ (\text{eV}),$$
$$x = 0 \text{ at the gate side.} \quad (42)$$

It is very difficult to account for this contribution to the noise present in the depletion region, since the latter is a function of the depletion region depth and profile. We estimate here the maximum barrier lowering that is obtained at the gate side of the region, at $x = 0$. Let us put $W = \alpha a$, with α a correcting parameter with a value close to 1. Using Eq. (B.2) (ε being the dielectric constant of Si):

$$\Delta U_{PF} \geqslant -\sqrt[4]{\frac{2\alpha e^3 n_{n_0} V_P}{\pi^2\varepsilon^3}}\ (\text{eV}). \quad (43)$$

For instance, for the case N_d equal 10^{16} atoms/cm^3 and $\alpha = 1$, ΔU results about -50 meV when $V_P = 1$ V, while it becomes -70 meV for $V_P = 5$ V, not totally negligible especially for shallow traps. From these considerations, it is

evident that the energy extracted from the noise measurements is always subjected to a systematic error, the measured value being less than the actual one.

An evident contribution of the Poole–Frenkel effect can be seen in studying the G–R noise given by dopants inside the channel of a Si-JFET at low temperatures. In this case it is possible to make a precise estimation since the Fermi level inside the channel is not affected by the applied field. This is because the channel is neutral and the current is due to drift. The electric field is therefore constant and ΔU_{PF} can be approximated by

$$\Delta U_{PF} \approx -\sqrt{\frac{e}{\pi\varepsilon}\frac{V_{DS}}{L}}\ (\mathrm{eV}). \tag{44}$$

For a gate length L of 1 μm the expected energy drop is about −22 meV when the applied voltage across the channel is 1 V, while for 2 μm of gate length the expected lowering is −15.5 meV. This effect seems small, but it must be compared with the energy of the dopants typically used in Si, which is 45 meV.

We do not consider in this paper the application of electric fields larger than the one considered above, which would lead to complete free-up of charge. This operating range was outside our experimental requirements. This subject deserves further study in a future paper.

7. Donor dopants as a source of G–R noise

Every type of trapping center, donor or acceptor, is a source of noise. Whether this noise is large or not depends on the time constant of the process, which is tied to the Fermi level and to the Fermi function. This rule applies also to dopants inside the channel of the transistor. Since their energy level is close to the conduction band the time constant of the trapping/de-trapping process is very short at ordinary temperatures: in other words, the donor dopants are ionized. Therefore, G–R noise from dopant atoms is not measurable at room temperature. The time constant associated with this type of trap remains small, down to less than 50 K. The noise effect is measurable due to the exponential increases of its amplitude as the temperature drops (Eq. (29)). For this reason for a long time it was believed that this 'anomalous' noise increase was due to high electric field or hot-electron effects [55,56]. Only after the work of Van der Ziel [32] was the source of this noise understood.

G–R noise around and below 10 K has already been investigated with Si-MOS transistors [57,58], which are able to work in this temperature range [59], as can be easily shown by applying the Poole–Frenkel effect to the electric field across the gate-oxide. Nevertheless, in MOSFETs the electrons in the channel have an energy profile different than in JFETs. For this reason, we tried to investigate the behavior of a Si-JFET at these very low temperatures of operation. As discussed in Section 5, we found a candidate for this experiment in the MX11CD JFET transistor from Moxtek, which has a large pinch-off voltage, coming from the large thickness of its conducting channel.

The only method used so far for investigating G–R noise from dopants was to measure the time constant of the process. We will show below that this is not necessary if an accurate mathematical model is adopted for this purpose. Our model is based on the very simple expression given in Eq. (29), where the trapping time constant is shown to depend mainly on the Fermi level within the channel. From that equation it is evident that a knowledge of the Fermi level dependence on temperature allows us to obtain a good fit of the measured data. In Appendix C the Fermi energy function is given down to low temperatures. If we consider the Fermi function for temperatures above 40 K, the noise results proportional to $\exp(2(E_c - E'_d)/K_B T)$, as already verified in the past [32]. This approximation is derived from the condition that $f_d \ll 1$ in this situation.

In the 3D-plot of Fig. 17, the noise for the JFET MX11CD is plotted from below 100 K down to 14 K. The noise at 14 K was close to 400 $\mathrm{nV}/\sqrt{\mathrm{Hz}}$, due to G–R noise from dopants. The very interesting fact can be seen that the Lorentzian frequencies are all found at higher frequencies than the upper measurement range of our instrument, except the one measured at 14 K, which was larger than 30 KHz. To fully account for the measured noise in the Fermi function f_d of Eq. (29)

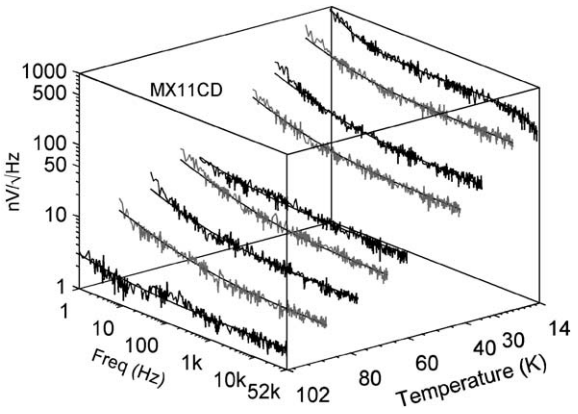

Fig. 17. The 3D-plot of the noise spectra measured for the JFET MX11CD in the temperature range 15–100 K. To each noise spectrum the fit is superimposed.

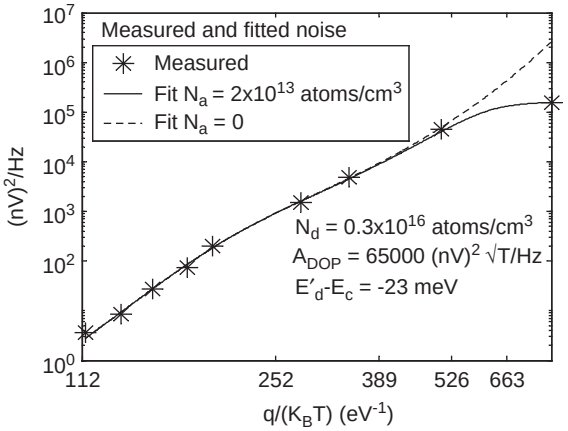

Fig. 18. Measured noise amplitude versus $1/T$ (*) for the MX11CD from 14 to 100 K. The continuous curve is the fit of the noise according to Eq. (45), while the dashed curve does not include the presence of compensated acceptors.

the Fermi energy was the one given in Eq. (C.1). Expression (C.1) for the Fermi energy has been obtained assuming that compensation acceptors are generally present inside the *n*-channel with a very small concentration. At ordinary temperatures their compensation effect is totally negligible, but when freeze-out occurs they become filled with electrons from dopants and cannot be neglected in the calculations. Therefore,

$$\overline{v_{\mathrm{nch}}^2} = \frac{A_{\mathrm{DOP}}}{\sqrt{T}} \frac{f_{\mathrm{d}}^2}{[1 - f_{\mathrm{d}} + 2g_{\mathrm{d}} f_{\mathrm{d}}][1 - f_{\mathrm{d}}^2]}. \tag{45}$$

The fitting parameters that we used were the amplitude A_{DOP}, the effective dopant energy level $E'_{\mathrm{d}} = E_{\mathrm{d}} + \Delta U_{\mathrm{PF}}$, the dopant concentration N_{d}, and the acceptor concentration N_{a}. In the above equation the term $\sqrt{T}$ comes from c_{n}, the capture probability rate, $c_{\mathrm{n}} = \sigma_{\mathrm{n}} v_{\mathrm{th}}$. In Eq. (45) the term dependent on the gate-to-source voltage and the pinch-off voltage, included in A_{DOP}, has been considered constant because of the small temperature dependence of the voltages in comparison to the other terms. The accuracy of the fitting function with respect to the measured data has been excellent, as can be seen for the continuous curve of Fig. 18. The extracted parameters were an amplitude A_{DOP} of about 65,000 $(\mathrm{nV})^2\ \sqrt{\mathrm{T}}/\mathrm{Hz}$, a donor concentration of about 0.3×10^{16} atoms/cm^3, a donor energy of $E'_{\mathrm{d}} - E_{\mathrm{c}} = -23$ meV, and a concentration of acceptors of 2×10^{13} atoms/cm^3.

The Poole–Frenkel effect plays an important role in the G–R noise from dopants. In the MX11CD channel the dopants are atoms of phosphorus, which have an ionization energy about 45 meV below the conduction band. In the above discussion we estimated ΔU_{PF} to be about –23 meV. The MX11CD is a JFET with a gate length between 1.5 and 2 μm. From Eq. (44) we expect a barrier lowering between −15 and −18 meV, which is quite close to the above extrapolation.

In Fig. 18 the fitting of the measured data is very good if a non-negligible acceptor compensation is considered. In the figure it is also plotted the case in which the compensation is assumed totally negligible (dashed curve). At the smaller temperatures the effect of the acceptor atoms is clearly seen.

From Eqs. (29)and (45) we derive

$$\sigma = \sqrt{\frac{m_{\mathrm{n}}}{3K_{\mathrm{B}}}} \frac{1}{A_{\mathrm{DOP}}} \frac{1}{Nd} 4e \frac{V_{\mathrm{GS}} - V_{\mathrm{T}}}{C_{\mathrm{GS}}} g_{\mathrm{d}}. \tag{46}$$

The MX11CD was operated at 1 mA of drain current and 1 V of drain to source voltage. The quantity $V_{\mathrm{GS}} - V_{\mathrm{T}}$ is estimated to be between 0.5 and 1 V at 14 K, while the capacitance C_{GS} is about 6 pF. From the above equation we can calculate σ to be between 5×10^{-16} and 1.15×10^{-16} cm^2. In Fig. 17 we have observed that

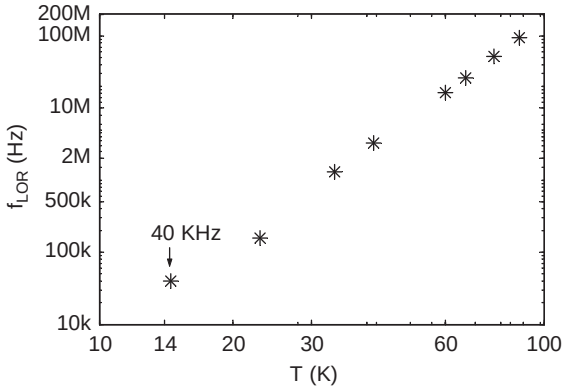

Fig. 19. Lorentzian frequencies versus temperature for the G–R noise from dopant atoms, after the parameters extracted from the data in Fig. 18.

for the lower temperature investigated the Lorentzian frequency is close to 33 KHz. From Eq. (30) and the estimated value for σ and the other parameters of interest, f_{LOR} can be extrapolated to be between 26 and 53 KHz, very close to the measured value. A plot of the Lorentzian frequencies versus temperature is shown in Fig. 19, where $V_{GS} - V_T$ is the average between the above-indicated values, or 0.75 V. As can be seen at 14 K, there is a good agreement with the measured value. It can be seen that above about 100 K the Lorentzian frequencies become very large, as expected. Below this temperature the Lorentzian frequencies are under 200 MHz. We are planning to perform an experiment where the frequency range for the measurements for the noise would be sufficient for this temperature interval, in order to prove further the theoretical interpretation we have discussed.

The obtained result proves that Si-JFET transistors cannot be used in low noise applications under 100 K, due to the strong effect of G–R noise from dopant atom sites.

8. Conclusions

Extensive measurements on the G–R noise of Si-JFET transistors from 14 K up to room temperature has been made on JFETs designed for low noise. It has been shown that around room temperature the main effect comes from deep level traps located in the middle between the valence and conduction bands. At the optimum temperature of operation for Si-JFETs, between 100 and 150 K, the energy of the traps responsible for G–R noise is around 0.1 eV from the band edges. By introducing a mathematical approximation, it was also possible to estimate the concentration of the G–R noise centers. For the very low noise processes that we measured we were able to reach a sensitivity of about 10^{-7} in the ratio between the trapping centers concentration and the dopant concentrations, N_T/N_d.

We were also able to measure the G–R noise coming from dopant atoms themselves inside the channel. From an accurate expression of the Fermi function, we were able to show that to obtain a good accuracy of the measured data, the effect of the possible presence of a compensated concentration of acceptors cannot be neglected at very low temperatures. We demonstrated that for applications that need low noise at very low temperatures the Si-JFET cannot be used at temperatures under about 100 K.

Acknowledgements

We thank Maurizio Perego for accurate layout of the boards used for noise characterization. We thank the staff of the Central Library of the Università della Bicocca for helping us in finding some of the papers and books text that we have used as references.

Appendix A. Proof of Eq. (11)

In this appendix, we solve Eq. (10). This differential equation can be transformed to the form

$$\frac{dy(t)}{dt} = -k_1 y(t) - k_2 y(t)^2 + h_A \delta(t). \tag{A.1}$$

To this aim we find a solution $n(t)$ that satisfy: $n(t) = \alpha + y(t)$, with $y(\infty) = 0$ and $\alpha > 0$, that gives the constraint that:

$$\alpha = \frac{-B + \gamma}{2C}, \quad \text{where } \gamma = \sqrt{B^2 + 4AC}. \tag{A.2}$$

With the above substitution Eq. (10) reduces to

$$\frac{dy(t)}{dt} = -\gamma y(t) - Cy(t)^2 + h_A\delta(t) \tag{A.3}$$

which is of form (A.1). It is convenient to seek for a solution of the form: $y(t) = f(t)1(t)$, where $f(t)$ is required to be continuous in $t = 0$. With this condition Eq. (A.3) becomes

$$f(0)\delta(t) + \frac{df(t)}{dt}1(t) = -\gamma f(t)1(t) - Cf(t)^2 1(t) + h_A\delta(t). \tag{A.4}$$

Now we put $z(t) = 1/f(t)$ and divide both terms of Eq. (A.4) by $f(t)^2$:

$$-z(0)\delta(t) + \frac{dz(t)}{dt}1(t) = \gamma z(t)1(t) + C1(t) - h_A z(0)^2\delta(t). \tag{A.5}$$

The terms proportional to $1(t)$ form a differential equation that can be solved if

$$z(t) = \beta_1 \exp(\gamma t) + \beta_2. \tag{A.6}$$

The function $z(t)$ given above is able to satisfies the whole Eq. (A.5) when

$$z(t) = \left(\frac{1}{h_A} + \frac{C}{\gamma}\right)\exp(\gamma t) - \frac{C}{\gamma}. \tag{A.7}$$

Namely

$$y(t) = \frac{1(t)}{\left(\frac{1}{h_A} + \frac{C}{\gamma}\right)\exp(\gamma t) - \frac{C}{\gamma}}. \tag{A.8}$$

The condition $n(t) = \alpha + y(t)$ together with the relation given in Eq. (A.2) and the above Eq. (A.8) gives the final:

$$n(t) = \frac{-B + \sqrt{B^2 + 4AC}}{2C} + \frac{1(t)}{\left[\frac{C}{\sqrt{B^2+4AC}} + \frac{1}{h_A}\right]\exp((\sqrt{B^2+4AC})t) - \frac{C}{\sqrt{B^2+4AC}}}. \tag{A.9}$$

Appendix B. Review of the main equations governing JFET operation

The operation of the JFET in the saturation region can be obtained starting from the Poisson equation, Eq. (21), which is valid for an abrupt junction where $p \gg n$. The boundary conditions are that at the gate, $x = 0$, the voltage is equal to V_G, while V_S should be the potential at the conducting channel boundary, $x = W$. In this respect it is assumed that the voltage at the drain, V_D, is close to V_S and the depletion region has a constant width W (see Fig. 3). The solution of the Poisson Eq. is therefore

$$V(x) = -\frac{1}{2}\frac{e}{\varepsilon}n_{n_0}(x - W)^2 + V_S + V_{bi}, \quad V(0) = V_G. \tag{B.1}$$

The built-in voltage V_{bi} is added to account for the fact that at zero bias the depletion region has a minimum width, due to the need to balance the diffusion current at the junction. From Eq. (B.1):

$$W = \sqrt{\frac{2\varepsilon}{en_{n_0}}[V_{bi} + V_S - V_G]} = a\sqrt{\frac{V_{bi} + V_S - V_G}{V_P}}. \tag{B.2}$$

The channel is completely pinched off when W equals the gate thickness a, or, assuming $V_S = 0$ for convenience, when

$$V_{bi} - V_{GOFF} = V_P = \frac{en_{n_0}a^2}{2\varepsilon} \quad \text{or} \quad V_{GOFF} = V_{bi} - V_P = V_T. \tag{B.3}$$

The pinch-off voltage, V_P, and the threshold voltage, V_T, are important parameters which characterize the JFET properties.

The current in the channel follows from Ohm's law:

$$I_{DS} = en_{n_0}Z(a - W)\mu E \approx en_{n_0}Z(a - W)\mu\frac{V_{DS}}{L}. \tag{B.4}$$

Namely

$$I_{DS} = en_{n_0}Za\left(1 - \sqrt{\frac{V_{bi} - V_G}{V_P}}\right)\mu\frac{V_{DS}}{L}. \tag{B.5}$$

Finally, the last parameter of interest is the transconductance g_m:

$$g_m \doteq \frac{dI_{DS}}{dV_G} = en_{n_0} Za\mu \frac{V_{DS}}{L}\left(\frac{1}{2\sqrt{V_P(V_{bi}-V_G)}}\right). \quad (B.6)$$

The last two equations can be given a more compact form that is valid whenever the channel current, I_{DS}, is much smaller than I_{DSS}, the drain current for the condition $V_{GS} = 0\,V$. For this case Eq. (B.5) can be expanded around $V_G = V_T$ giving

$$I_{DS} = en_{n_0} Za\mu \frac{V_{DS}}{L}\frac{1}{2}\frac{V_G - V_T}{V_P}. \quad (B.7)$$

Consequently, the transconductance, g_m, can be expressed as

$$g_m = en_{n_0} Za\mu \frac{V_{DS}}{L}\frac{1}{2}\frac{1}{V_P} \quad (B.8)$$

or

$$\frac{I_D}{g_m} = V_G - V_T. \quad (B.9)$$

Appendix C. The Fermi energy in a semiconductor

In an n-type semiconductor there is always a certain degree of compensation due to the presence of acceptors. The effects of these dopants can be very small and totally negligible at ordinary temperatures. At cryogenic temperatures this is not the case and electrons tend to fill, or freeze out, at both the n-type and the p-type dopant atoms. So the actual concentration of electrons in the conduction band satisfy the condition $n + N_{a-}(T) = (N_d - n_d)$, where $N_{a-}(T)$ represents the concentration of acceptor centers that are not filled, $N_{a-}(300) \approx 0$ while $N_{a-}(0) \approx N_a$. This compensation effect is negligible at ordinary temperatures, but it is effective under about 40 K [60]. This has been taken into account in deriving the fitting of the noise measurements at the lower temperatures. After a few calculations, the Fermi level can be expressed by

$$E_F = E_c - K_B T \ln\left\{\frac{N_c}{N_d}\frac{1+gz/y}{2(1-z)} \times \left[1+\left(1+\frac{4gy(1-z)}{(y+gz)^2}\right)^{1/2}\right]\right\}. \quad (C.1)$$

where

$$y = \frac{N_C}{N_d}\exp\left(\frac{E_d - E_C}{K_B T}\right), \quad z = \frac{N_{a-}(T)}{N_d}. \quad (C.2)$$

In Eq. (C.1) there is a dependence on temperature of z that complicates the final expression. To simplify it is convenient to consider $N_{a-}(T) = N_a$ for temperatures lower than about 40 K and $N_{a-}(T) = 0$ above that range. For $T > 40\,K$ Eq. (C.1) simplifies to

$$E_F = E_c - K_B T \ln\left\{\frac{N_c}{N_d}\frac{1}{2}\left[1+\left(1+\frac{4g_d}{y}\right)^{1/2}\right]\right\}. \quad (C.3)$$

In addition, in the case that N_d is sufficiently small compared to N_C ($4g_d/y \approx 0$) from above we can obtain the classical expression:

$$E_F = E_c - K_B T \ln\left(\frac{N_c}{N_d}\right). \quad (C.4)$$

References

[1] R.C. Jones, J. Opt. Soc. Am. 43 (1953) 1.
[2] A. Alessandrello, J.W. Beeman, C. Brofferio, O. Cremonesi, E. Fiorini, A. Giuliani, E.E. Haller, A. Monfardini, A. Nucciotti, M. Pavan, G. Pessina, E. Previtali, L. Zanotti, Phys. Rev. Lett. 82 (1999) 513.
[3] A. Alessandrello, C. Brofferio, C. Cattadori, R. Cavallini, O. Cremonesi, L. Ferrario, A. Giuliani, B. Margesin, A. Nucciotti, M. Pavan, G. Pessina, G. Pignatel, E. Previtali, M. Sisti, J. Phys. D 32 (1999) 3099.
[4] K.K. Wang, A. van der Ziel, E.R. Chenette, IEEE Trans. Electron Devices ED-22 (1975) 591.
[5] P.F. Manfredi, L. Ratti, V. Re, V. Speziali, IEEE Trans. Nucl. Sci. NS-46 (1999) 1294.
[6] F.N. Hooge, IEEE Trans. Electron Devices ED-41 (1926–1935).
[7] S. Christensson, I. Lundstrom, C. Svensson, Solid-State Electron. 11 (1968) 797.
[8] S. Christensson, I. Lundstrom, Solid-State Electron. 11 (1968) 813.

[9] E. Simoen, C. Claeys, Solid-State Electron. 39 (1996) 949.
[10] E. Simoen, C. Claeys, Solid-State Electron. 43 (1999) 865.
[11] N. Lukyanchikova, N. Garbar, M. Petrichuk, E. Simoen, C. Claeys, Solid-State Electron. 44 (2000) 1239.
[12] W. Shockley, W.T. Read Jr., Phys. Rev. 87 (1952) 835.
[13] G. Bemski, Proc. IRE 46 (1958) 990.
[14] W. Shockley, Proc. IRE 46 (1958) 973.
[15] K. Kandiah, M.O. Deighton, F.B. Whiting, J. Appl. Phys. 66 (1989) 937.
[16] K. Kandiah, IEEE Trans. Electron Devices ED-41 (1994) 2006.
[17] M.J. Uren, D.J. Day, M.J. Kirton, Appl. Phys. Lett. 47 (1985) 1195.
[18] E. Gatti, A. Longoni, R. Sacco, J. Appl. Phys. 78 (1995) 6283.
[19] F.N. Hooge, L. Ren, Physica B 193 (1994) 31.
[20] S. Machlup, J. Appl. Phys. 25 (1954) 341.
[21] A.D. Van Rheenen, G. Bosman, C.M. van Vliet, Solid-State Electron. 28 (1985) 457.
[22] C.T. Sah, Proc. IRE 52 (1964) 795.
[23] P.O. Lauritzen, Solid State Electron. 8 (1965) 41.
[24] L.D. Yau, C.T. Sah, IEEE Trans. Electron Devices ED-16 (1969) 170.
[25] K.K. Hung, P.K. Ko, C. Hu, Y.C. Cheng, IEEE Trans. Electron. Devices 37 (1990) 654.
[26] R.A. Smith, Semiconductors, 2nd Edition, Cambridge University Press, Cambridge, 1978, pp. 282–283.
[27] R.E. Burgess, Physica XX 11 (1954) 1007.
[28] R.E. Burgess, Proc. Phys. Soc. B 68 (1955) 661.
[29] M. Lax, Rev. Modern Phys. 32 (1960) 25.
[30] R.E. Burgess, Proc. Phys. Soc. B 69 (1956) 1020.
[31] F.N. Hooge, L. Ren, Physica B 191 (220–226).
[32] A. Van der Ziel, Proc. IEEE 51 (1963) 1670.
[33] D.C. Murray, A.G.R. Evans, J.C. Carter, IEEE Trans. Electron Devices ED-38 (1991) 407.
[34] F. Scholz, J.M. Hwang, D.K. Schroder, Solid-State Electron. 31 (1988) 205.
[35] SKUDOTECH® is a Registered trademark by SELITE, Via Aurelio Saffi 29, 20123 Milano, IT.
[36] A. Alessandrello, C. Brofferio, O. Cremonesi, A. Giuliani, A. Monfardini, A. Nucciotti, M. Pavan, G. Pessina, E. Previtali, IEEE Nucl. Sci. NS-47 (2000) 1851.
[37] E.A. Hendriks, R.J.J. Zijlstra, Physica 147B (1987) 291.
[38] S. Kugler, IEEE Trans. Electron Devices ED-35 (1988) 623.
[39] V. Grassi, C.F. Colombo, D.V. Camin, IEEE Trans. Nucl. Sci NS-48 (2001) 2899.
[40] K. Kandiah, F.B. Whiting, Nucl. Instr. and Meth. A 326 (1993) 49.
[41] K. Kandiah, F.B. Whiting, Nucl. Instr. and Meth. A 305 (1991) 600.
[42] K. Kandiah, F.B. Whiting, Solid-State Electron. 21 (1978) 1079.
[43] A.D. van Rheenen, G. Bosman, R.J.J. Zulstra, Solid-State Electron. 30 (1987) 259.
[44] F.J. Scholz, J.W. Roach, Solid-State Electron. 35 (1992) 447.
[45] J.W. Haslett, E.J.M. Kendall, IEEE Trans. Electron Devices ED-19 (1972) 943.
[46] W.H. Press, B.P. Flannery, S.A. Teukoslsky, W.T. Vetterling, Numerical Recipes in C++, Cambridge University Press, Cambridge, 2002, pp. 704–711.
[47] D.V. Camin, C.F. Colombo Grassi, J. Phys. IV (Proceedings) 12 (2002) Pr3–37.
[48] A. Fascilla, G. Pessina, Nucl. Instr. and Meth. A 469 (2001) 116.
[49] M.W. Lund, K.W. Decker, R.T. Perkins, J.D. Phillips, Nucl. Instr. and Meth. A 380 (1996) 318.
[50] A. Alessandrello, C. Brofferio, O. Cremonesi, A. Fascilla, A. Giuliani, Mark W.Lund, A. Nucciotti, M. Pavan, G. Pessina, E. Previtali, Low noise silicon JFETs working at low temperatures for bolometric detector readout, 'WOLTE 4, 4th European Workshop on Low Temperature Electronics' 2000, pp. 137–141.
[51] J.W. Haslett, E.J. Mkendall, F.J. Scholz, Solid-State Electron. 18 (1975) 199.
[52] F.J. Morin, J.P. Maita, Phys. Rev. 96 (1954) 28.
[53] C. Jacoboni, C. Canali, G. Ottavaini, A. Alberigi Quaranta, Solid-State Electron. 20 (1977) 77.
[54] A. Van Der Ziel, Fisica dei dispositivi elettronici a stato solido, III Edizione, Liguori Editore, 1979, pp. 554–556 (translation from Solid State Physical Electronics, Prentice-Hall, Englewood Cliffs, NJ).
[55] K. Takagi, K. Matsumoto, Solid-State Electron. 20 (1977) 1.
[56] F.M. Klassen, J.R. Robinson, IEEE Trans. Electron Devices ED-17 (1970) 852.
[57] R. Jayaraman, C.G. Sodini, IEEE Trans. Electron Devices ED-36 (1989) 1773.
[58] B. Dierickx, E. Simoen, S. Cos, J. Vermeiren, C. Claeys, G.J. Declerck, IEEE Trans. Electron Devices ED-38 (1991) 907.
[59] B. Lengeler, Cryogenics 40 (1974) 439.
[60] M. Shur, Physics of Semiconductor Devices, Prentice-Hall, Englewood Cliffs, NJ, 1990, pp. 54–66.